Construction and Building Materials 93 (2015) 1022–1033

Contents lists available at ScienceDirect

Construction and Building Materials

journal homepage: www.elsevier.com/locate/conbuildmat

Mechanical response of fiber reinforced concrete overlays over asphalt concrete substrate: Experimental results and numerical simulation

F. Isla [a,*], B. Luccioni [a], G. Ruano [a], M.C. Torrijos [b], F. Morea [b], G. Giaccio [c], R. Zerbino [b]

[a] CONICET, Structures Institute, National University of Tucumán, Argentina
[b] CONICET, LEMIT, Engineering Faculty, National University of La Plata, Argentina
[c] CIC, LEMIT, Engineering Faculty, National University of La Plata, Argentina

HIGHLIGHTS

- A new experimental method for the assessment of pavement whitetopping is proposed.
- Substrate-fiber concrete reinforced overlay composite beams are tested under flexure.
- Concrete overlays reinforced with steel fibers and synthetic fibers are compared.
- Numerical analysis of the structural behavior of the composite beams is presented.
- FRC overlay effect is comparatively greater for asphalt substrates than for concrete.

ARTICLE INFO

Article history:
Received 10 November 2014
Received in revised form 15 April 2015
Accepted 2 May 2015
Available online 18 May 2015

Keywords:
Fiber reinforced concrete
Overlay
Whitetopping
Pavement reinforcement
Numerical model
Composite
Fibers pull-out

ABSTRACT

Fiber reinforced concrete overlays are nowadays an alternative for repairing and reinforcing pavements. The contribution of concrete overlays strongly depends on the bond with the substrate. The fibers help sewing contraction joints and eventual cracks and, in this way prevent the propagation of cracks along the substrate–overlay interface. Therefore, the addition of fibers to the overlay allows reducing repair thickness, increasing service life and improving pavements general performance.

Some experimental tests performed for the development of a method to assess different fibers efficiency in this type of applications are presented in this paper. Substrate–overlay composite beams are tested under flexure. The beams consist of overlays of plain and fiber reinforced concretes, containing steel and macro-synthetic fibers, applied over an asphalt concrete substrate. The numerical simulation of the beams is also included in the paper. Fiber reinforced concrete is considered as a composite material made of a concrete matrix and fibers and its mechanical behavior is modeled with a simple homogenization approach based on modified mixture theory. The numerical simulation can accurately reproduce material characterization tests and predict the bearing capacity of the composite beams. Furthermore, other substrate/overlay alternatives are numerically studied. The numerical results could be useful to improve the design of these intervention techniques.

1. Introduction

A common way to restore the performance level of a deteriorated pavement is through a superficial reinforcement called overlay. The whitetopping overlays are made of portland cement concrete. They are classified in unbonded and bonded whitetopping. Overlays laid on old asphalt pavements presenting high deterioration (e.g. severe rutting, potholes, alligator cracking, subgrade/subbase issues, shoving, and pumping) should be considered as unbonded overlays. On the contrary, if the asphalt pavement is in fair or better structural condition with typical distresses (e.g. rutting, shoving, slippage, and thermal cracking) the overlay can be considered as a bonded one [1]. No adherence with the old pavement is assumed for unbonded overlays. The design procedure does not consider any structural contribution from the old pavement (see Fig. 1a) and thus, a thicker reinforcement (normally 100–280 mm) is obtained. The overlay performs as a new pavement, and the existing one provides a stable base [1]. The reinforcement thickness can be reduced (50–100 mm) in case of

* Corresponding author at: CONICET, Structures Institute, National University of Tucumán, Av. Independencia 1800, 4000 S.M. de Tucumán, Argentina. Tel.: +54 381 4364087.
E-mail address: fisla@herrera.unt.edu.ar (F. Isla).
URL: http://www.herrera.unt.edu.ar/iest (F. Isla).

http://dx.doi.org/10.1016/j.conbuildmat.2015.05.050
0950-0618/

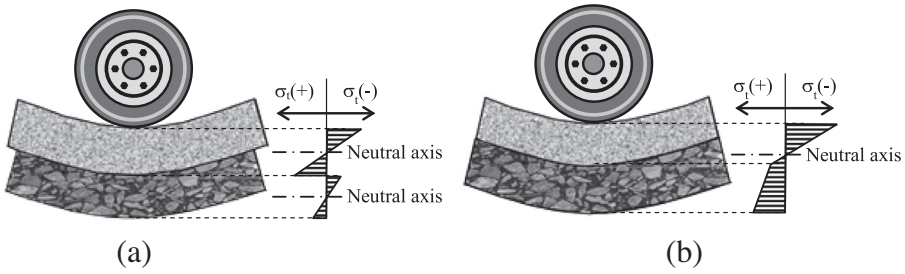

Fig. 1. Strains in repaired pavement. (a) Unbonded overlay and (b) bonded overlay.

bonded overlays because both the substrate and the overlay can be assumed to work together (see Fig. 1b) as a monolithic pavement [2]. However, the adherence obtained during the construction phase is gradually reduced along time [3] due to many reasons such as shear stress concentration at the interface due to tension cracking of the overlay, adverse conditions during road construction (e.g. oil stains), inadequate superficial roughness of the overlay, among others. The bonded concrete overlay of asphalt pavements mechanistic empirical design guide (BCOA-ME) [4] has been developed to calculate Portland cement concrete overlay thickness based on climate parameters, existing structural parameters, as well as asphalt and concrete material properties.

According to Turatsinze et al. [5], the main reasons that produce loss of adherence are: external mechanical loads and length changes between substrate and overlay. In both mechanisms, this lack of adherence begins primarily in reinforcement disruptions, edges, cracks and joints.

The effect of loads on the reinforced pavement can be observed in Fig. 2. Under the wheel load, some parts of the overlay may result subjected to tensile stresses. Due to the different responses of the concrete overlay and the asphalt substrate, these tension stresses in coincidence with a joint or a crack, may promote the debonding between substrate and overlay. The cyclic load effects contribute to the crack growth along the interface. Temperature change produces differential length variations that promote cracking of the overlay and shear stress concentrations at the substrate–overlay interface contributing to the debonding.

Fiber reinforced concrete (FRC) overlay is an attractive alternative because fibers can transfer stresses through the cracks, reducing mechanical discontinuities and shear stresses at the interface. Prevention of reinforcement layer debonding due to the addition of fibers have also been observed by the authors in other FRC repairing and reinforcing tests [6]. In general, fibers allow reduction of the overlay thickness, increment the service life and the overall performance of the structure.

Although FRC whitetopping have been used during the last decade, the benefits of fibers addition cannot be properly quantified nowadays. Many researchers have studied FRC overlay focusing on the substrate–overlay interface bonding [7–11]. Turatsinze and Tran ([7–9]) analyzed the flexural response of FRC overlay over plain concrete and steel beam substrates. Their main conclusions were: (a) the interlocking mechanism governs the overlay cracking and the crack propagation at the interface, (b) drying shrinkage affects the crack initiation and propagation rate in the overlay that reduces its durability and (c) a lower stiffness and a higher resistance of the overlay promotes adherence and durability of the interface. Also, monotonic flexural tests do not show all the positive aspects of incorporating fibers into FRC overlay. The fibers, even at low dosage, are capable of transferring loads, limiting crack propagation and improving the fatigue response with respect to plain concrete. Tayeh et al. [11] show the importance of an optimal preparation of the interface to obtain a better mechanical bonding in the compound. Perez et al. [10] indicated that improvement in roughness and adherence between overlay and substrate not always guarantee a monolithic response of the composite and over a certain level of roughness, the risk of bond loss increases.

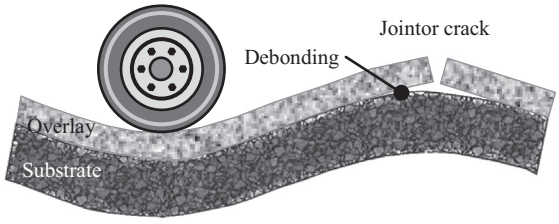

Fig. 2. Debonding produced by traffic loads.

Since 2004, FRC has been used in road applications for construction of thin and ultrathin whitetopping overlays [12]. Cervantes and Roesler [13] show that macrofibers increase the reinforcement fatigue life due to the higher capacity and efficiency in load transfer. Bordelon and Roesler [14] developed a design method for ultrathin whitetopping where the contribution of fiber can be significantly appreciated.

This paper evaluates the effect of fibers in flexural response of composite substrate–overlay beam specimens with the objective of comparing the effects of incorporating different types and contents of fibers to the overlay assuming perfect bonding.

A plain concrete and two fiber reinforced concretes overlays were molded over an asphalt concrete substrate to analyze their response. The paper is completed with the numerical simulation of the composite beams under flexure that allows understanding how they work and the effect of adding different fibers to the overlay, the role of the existing substrate and the effect of temperature on the behavior of the composite structure.

2. Experimental program

2.1. Methodology

To evaluate the overlay–substrate mechanical response a three point bending test over a span of 350 mm was adopted. Prismatic specimens 400 mm long, 100 mm width and 100 mm height were used. They were composed of two layers of 50 mm thickness each, an asphalt concrete substrate and a Portland cement concrete overlay.

The composite beams were prepared by molding $300 \times 400 \times 50\ mm^3$ slabs with asphalt concrete following EN 12697-33 [15]. The slabs were cut, obtaining three 100 mm width prisms and concrete was poured over them (Fig. 3).

Three composite beams for each type of concrete overlay were tested. The beams were placed with the asphalt concrete substrate in the compression zone and the overlay in the tension zone (Fig. 4a), simulating the effect of the transit loads shown in Fig. 2. A 10 mm notch was cut in the overlay in the middle of the span to localize the failure. A clip gage, that registered the crack mouth aperture (CMOD), controlled the tests (Fig. 4a). An initial displacement rate of 0.05 mm/min was established and once the crack aperture reached 0.3 mm, the displacement rate was increased to 0.2 mm/min. Considering that some cracks might develop along the interface, the relative vertical displacement between two points located at both sides of the substrate–overlay interface was measured with a LVDT (Fig. 4a).

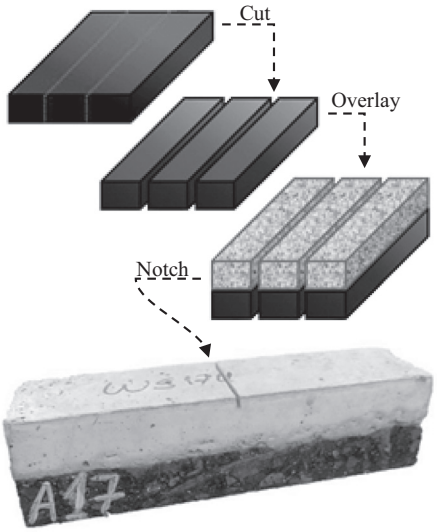

Fig. 3. Composite beams.

Mechanical properties of the substrate and the overlay were measured at the same age of the composite beams tests.

Overlays compressive strength and modulus of elasticity were measured by conventional tests on $d = 100$ mm, $h = 200$ mm cylinders. The flexure response was evaluated following the general guidelines of the EN14651 standard [16]; small beams, similar in size to the composite beams: 105 mm height, 75 mm width and 430 mm long, with a 18 mm depth notch, were adopted. These specimens were tested under three points bending over a 350 mm span. In this way, the composite beams and the FRC beams tested under similar load arrangement can be compared. The first peak strength (f_L), the maximum flexural strength (f_M) and the residual strengths f_{R1}, f_{R2}, f_{R3} and f_{R4} were calculated for the FRC beams. These last values represent the nominal strength capacity for 0.5, 1.5, 2.5 and 3.5 mm crack openings respectively. The length/height and the notch/height ratios remained the same as the values established in the EN14651 [16] standard. To calculate the residual strengths for the same rotations considered in the standard the CMOD limits were corrected, as it is explained in Ref. [17].

For the asphalt concrete substrate characterization, traditional tests in road engineering were carried out; dynamic modulus, Marshall stability and direct tensile strength. As the substrate would be compressed in bending tests, compression tests were also developed. In this case, the axial strains were measured with two LVDT on the lateral opposite sides of the specimens (Fig. 4b). The applied axial deformation rate was similar to the deformation rate that would suffer the substrate in the composite beam flexure test. Based on the strain measurements, a "static modulus of elasticity" was calculated in accordance with the criteria used in concrete but without loading cycles.

2.2. Materials and mixtures

Composite beams were made using three overlays with different post peak response, all of them with the same base concrete: the plain concrete (PC), a FRC with 3 kg/m^3 (0.33% in volume) of macro-synthetic fibers (MFRC) 60 mm length and 0.62 mm diameter, and a FRC with 40 kg/m^3 (0.50% in volume) of hooked-end steel fibers (SFRC) 35 mm length and 0.55 mm diameter. The respective composite beams are identified as PC-A, MFRC-A and SFRC-A. To ensure the proper filling of the molds a self-compacting type mixture was used as base concrete for the overlays. It was prepared using ordinary Portland cement, calcareous fine powder and fly ash as fine powder, natural siliceous sand, granitic crushed stone of 12 mm maximum size, and a polycarboxylate based superplasticizer. The slump flow diameters were 725 mm, 680 mm and 695 mm for PC, MFRC and SFRC respectively.

The substrate (A) was a hot mix asphalt; it was made with conventional asphalt binder (penetration of 47 mm, softening point of 54.8 °C and a cinematic viscosity at 60 °C of 3350 dPa s), two coarse aggregates (6–20 mm and 6–12 mm), fine aggregate (0–6 mm) and lime. It was designed using the Marshall method resulting an optimum asphalt content of 5%, a design density of 2.389 g/cm^3 and 4.1% of air voids. Table 1 shows the proportions of the mixtures.

2.3. Overlays and substrate properties

The compressive strength and the elasticity modulus of the PC were 37.3 MPa and 27.2 GPa, respectively. In the case of the FRC the values of compressive strengths and elasticity modulus were 33.0 MPa and 26.4 GPa and, 38.0 MPa and 26.1 GPa for MFRC and SFRC, respectively.

Three beams of each type of concrete (PC, MFRC, SFRC) used as overlay were subjected to three point bending tests. Fig. 5 shows average load-CMOD curves and standard deviation obtained for the three point bending tests of each type of concrete. The vertical segments in Fig. 5 indicate standard deviation for f_L, f_{R1}, f_{R2}, f_{R3} and f_{R4}. Mean stress values are presented in Table 2. The first peak strength f_L was similar in the three cases because this stress depends on the strength of the plain concrete. The different behavior of the FRC can be distinguished through the values of the maximum strength and the residual strengths. SFRC has hardening response, while in MFRC the loading capacity decreased after the first peak until a residual stress of approximately 30% of the f_L. The residual capacity of plain concrete is negligible.

Regarding the substrate, the asphalt mixture has 7453 MPa dynamic modulus at 20 °C, 15.3 kN Marshall stability, 1448 kPa indirect tensile strength, 2.3 MPa compressive strength and 1.5 GPa static elasticity modulus. A surface texture with a typical roughness of asphalt concrete pavements was obtained.

2.4. Test results and analysis

Fig. 6a compares average load-CMOD curves and standard deviation (vertical segments) obtained for composite beams PC-A, MFRC-A and SFRC-A. The behavior of the composite beam PC-A is similar to the behavior of plain concrete (see PC, Fig. 5). In the MFRC-A beams, after the matrix cracks, the residual load capacity grows progressively until almost a 70% of the first crack load, instead of remaining constant like in the MFRC (see Fig. 5). These improvements in the load residual capacity of the composite beam can be associated to cracks difficulty to go inside

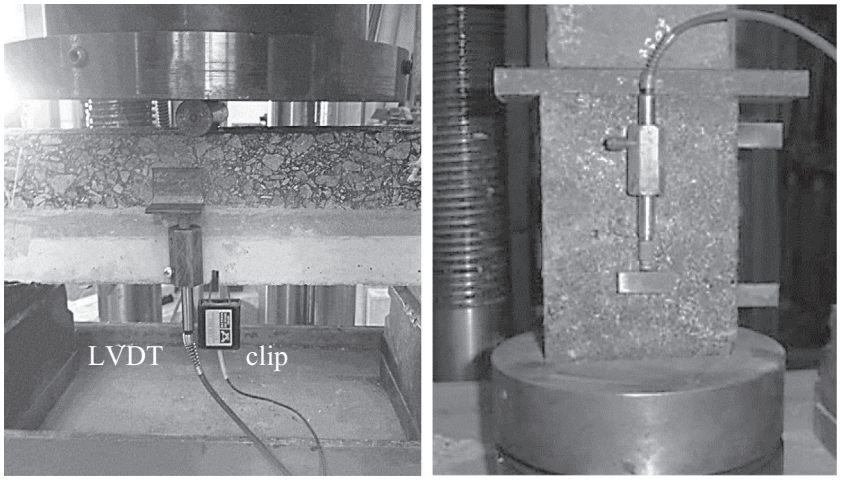

Fig. 4. (a) Substrate–overlay beams bending test. (b) Asphalt concrete compression test setup.

Table 1
Mix proportions.

Concrete overlays				Asphalt concrete substrate	
Materials (kg/m^3)	PC	MFRC	SFRC	Materials (%)	A
Water		157		Asphalt binder	5.0
Portland cement		259		Coarse aggregate 6–20 mm	23.7
Fine powder		175		Coarse aggregate 6–12 mm	28.5
Natural sand		735		Crushed sand 0–6 mm	40.9
Coarse aggregate		865		Lime	1.9
Superplasticizer		2.5			
Macro-synthetic fibers	–	3	–		
Steel fibers	–	–	40		

the substrate. The described behavior differs from the one observed when a macro-synthetic fiber overlay was applied over a concrete substrate. In this case, in previous experiences [18], no increase in the load capacity was obtained during the postpeak regime. The behavior of the composite SFRC-A beams was similar to the one of its respective concrete (SFRC, Fig. 5). The residual response was better than the one observed in previous studies using the same type and content of steel fibers but on concrete substrates. In general, it is possible to infer that the FRC residual capacity is increased when more deformable substrates (i.e. asphalt concrete substrate instead of concrete substrate) are reinforced and when the bond strength delay the crack propagation along the interface.

The average relative vertical displacements registered by the LVDTs in the interface region as a function of CMOD are plotted in Fig. 6b. Initially, the LVDT presents compressive displacements (shortens) until the first peak load is reached (see Fig. 6a), after that, and when an important crack opening takes place in the overlay, the LVDT starts to recover its length but without elongation. In the PC-A beams, when the load starts to decrease, only a slight change in the deformation of the LVDT takes place. It starts to deform rapidly when the load decreases below 500 N (CMOD near 0.264 mm). For MFRC-A beam, the LVDT starts to recover more gradually when the minor postpeak load is reached (CMOD larger than 0.295 mm). Finally, for SFRC-A beams, the recovery of the LVDT displacements starts for a crack opening of approximately 1.690 mm.

Although the observed behavior does not seem to be associated to a bond loss between the substrate and the overlay, in some cases it was observed that the cracks run out of the overlay. They propagate to the substrate–overlay interface and then they run into the asphalt concrete substrate and continue propagating (Fig. 7).

Table 3 presents the residual load capacities of both the composite and the overlay concrete beams expressed as relative values of the first peak load (L_L). The residual loads, were determined following the EN 14651 [16] standard, and the maximum loads are: L_{R1}, L_{R2}, L_{R3}, L_{R4} and L_M, respectively. Relative residual capacities are greater for the composite beams than for each overlay concrete. This difference is more pronounced in the case of MFRC-A composite beams, where the relative residual capacity is almost twice the relative residual capacity of the MFRC beam. For SFRC-A composite beams, the increase in the relative residual capacity with respect to SFRC beams is lower (approximately 40%) than that found for MFRC.

To determine the effect of surface roughness on the flexural response of the layered beams, possible enhancements of the testing setup considering weak substrate–overlay interface should be considered in the future.

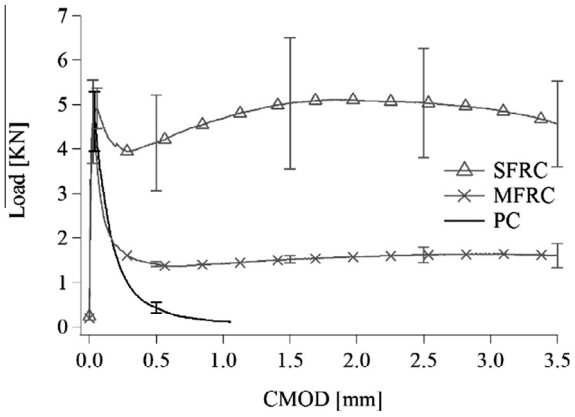

Fig. 5. Average load-CMOD curves for the concretes used as overlays.

3. Numerical models

3.1. Introduction

FRC is increasingly used for repairing or strengthening purposes nowadays. Although some experimental papers related to the retrofitting of reinforced concrete structures with FRC have been published [19,20], practical tools for the design of these techniques are still being developed. Predicting the response of retrofitted structures requires the numerical simulation of the resulting composite structures.

While concrete and reinforced concrete behavior under multi-axial loads has been well studied, documented and modeled by several researchers, several differences between the constitutive models proposed for FRC in the existing codes can be found [21].

A simple homogenization approach for SFRC based on a modified mixture theory was proposed by the authors in a previous paper [22]. SFRC is considered a composite material composed of a concrete matrix, which is modeled with an elastoplastic model [23,24], and steel fibers considered orthotropic elastoplastic inclusions that can debond and slip from the matrix. Constitutive equations of fibers are modified using the approach proposed by Luccioni and López [25] to include this inelastic phenomenon without explicitly modeling the interface. The model requires concrete properties, fibers material, geometry, distribution and orientation as input data. The fibers bond–slip behavior is obtained from pull-out tests.

This model is used to simulate the mechanical response of FRC beams and composite beams.

3.2. Constitutive models

FRC can be regarded as a composite material consisting of a brittle concrete matrix plus short disperses fibers. One simple way of modeling composites behavior is mixture theory. This paper employs modified mixture theory for orthotropic materials to simulate FRC behavior taking into account the concrete and fibers contribution. Particularly, the anisotropic behavior of fibers and their slippage are modeled in a simplified way [22].

The classic theory of mixtures [26] assumes that all components in the composite have the same strain (compatibility condition). If fiber/matrix interface is not explicitly considered and fibers are supposed to be oriented in n directions, this condition is written as:

$$(\varepsilon_{ij})_{FRC} = (\varepsilon_{ij})_{Conc} = (\varepsilon_{ij})_{Fi} \tag{1}$$

where ε_{ij}, $(\varepsilon_{ij})_{Conc}$, $(\varepsilon_{ij})_{Fi}$ with $i = 1, 2, \ldots, n$ are the strain tensors for the composite (FRC), concrete and fibers in i-direction respectively.

On the other hand, the composite free energy density can be written:

$$\Psi(\varepsilon_{ij}, \alpha_i) = \sum_{m=1}^{n} k_m \Psi_m\left(\varepsilon_{ij}, (\alpha_i)_m\right) \tag{2}$$

where $\Psi_m(\varepsilon_{ij}, (\alpha_i)_m)$ is the free energy density per volume unity of each m-component, $k_m = dV_m/dV$ is the corresponding volumetric ratio and $(\alpha_i)_m$ is a set of internal variables.

Table 2
Strength and residual stress parameters of the different concrete used as overlays.

Concretes	f_L (MPa)	f_M (MPa)	f_{R1} (MPa)	f_{R2} (MPa)	f_{R3} (MPa)	f_{R4} (MPa)
PC	4.7	4.7	0.7	0.1	–	–
MFRC	4.8	4.8	1.6	1.5	1.6	1.7
SFRC	5.0	5.6	4.0	4.8	5.1	5.1

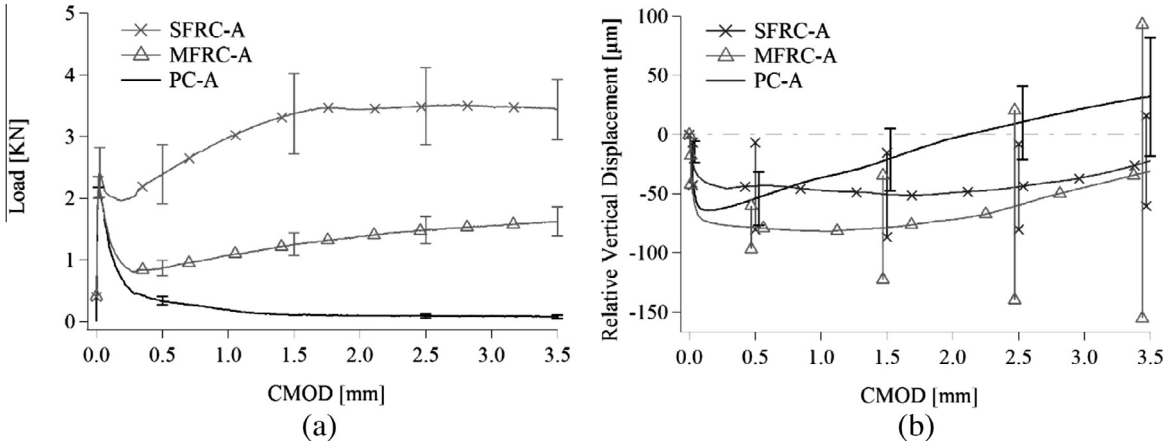

Fig. 6. Bending tests on composite beams; (a) average load-CMOD curves; (b) average relative vertical displacement-CMOD curves.

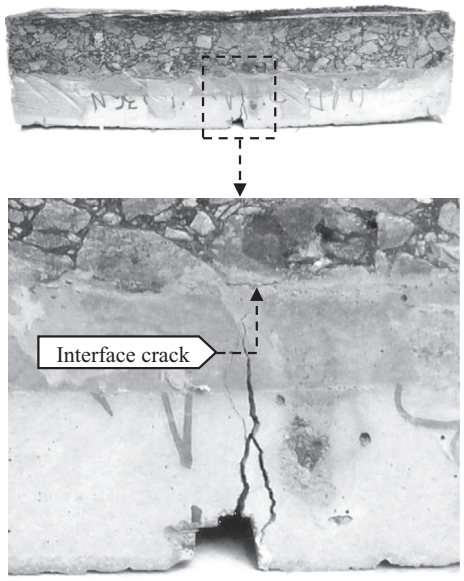

Fig. 7. Specimen detail after test.

The composite secant constitutive equation can be obtained from Coleman relations that guarantee the fulfillment of Clausius–Duhem inequality [27]:

$$\sigma_{ij} = \frac{\partial \Psi(\varepsilon_{kl}, \alpha_k)}{\partial \varepsilon_{ij}} = \sum_{m=1}^{n} k_c \frac{\partial \Psi_c(\varepsilon_{kl}, \alpha_{kc})}{\partial \varepsilon_{ij}} = \sum_{m=1}^{n} k_m (\sigma_{ij})_m \tag{3}$$

where each component stress $(\sigma_{ij})_m$ is obtained from the constitutive equations respectively.

Table 3
Residual load capacity of composite beams and overlay beams (relative values of the first peak load).

	L_L	L_M	L_{R1}	L_{R2}	L_{R3}	L_{R4}
Composite beams: concrete overlay-asphalt concrete substrate						
PC-A	1	1	0.20	0.08	0.05	0.05
MFRC-A	1	1	0.38	0.50	0.59	0.67
SFRC-A	1	1.44	0.89	1.24	1.41	1.43
Overlays: plain concrete and fiber reinforced concrete beams						
PC	1	1	0.15	0.02	0.00	0.00
MFRC	1	1	0.33	0.31	0.33	0.35
SFRC	1	1.12	0.80	0.96	1.02	1.02

Note that Eq. (1) is a strong restrain. Fiber slipping over the matrix plays an important role in FRC behavior, especially in post-cracking behavior. Therefore, Eq. (1) is retained but the fibers constitutive model is modified to account slipping [22,25,28] without explicitly modeling the interface. The fibers total strain represents both the fibers and the interface strains and it is formed by an elastic strain $(\varepsilon^e_{ij})_{Fi}$, a plastic strain $(\varepsilon^p_{ij})_{Fi}$ and a slipping strain $(\varepsilon^s_{ij})_{Fi}$:

$$(\varepsilon_{ij})_{Fi} = \left(\varepsilon^e_{ij}\right)_{Fi} + \left(\varepsilon^p_{ij}\right)_{Fi} + \left(\varepsilon^s_{ij}\right)_{Fi};\ i = 1, 2, \ldots, n \tag{4}$$

Strictly, only the two first terms take place in fibers, the third term corresponds to inelastic fiber-matrix relative displacement that takes place at the interface. As a result of Eqs. (1) and (4), the strain in the fibers is not actually equal to that in the matrix.

Both plasticity and inelastic slipping phenomena are modeled using an orthotropic elastoplastic model. Normally, fibers slip before yielding, so the elastic threshold actually represents the slipping threshold. This threshold is markedly lower in fibers direction and slipping is only allowed in fibers direction.

Space mapping approach [23,29] is used in order to account this orthotropy without defining orthotropic criteria for slipping threshold. This approach assumes that there are two spaces, the actual orthotropic space and the fictitious isotropic space. Stress tensors in both spaces are related through a linear transformation defined by a fourth order stress mapping tensor that depends on material orthotropy. The problem is solved in the fictitious isotropic space and then the results are mapped to the actual orthotropic space. Von Mises yield criterion is used to define the slipping threshold and slipping flaw in the fictitious isotropic space. Force–displacement curves obtained from pull-out tests define slipping hardening in fibers direction in the case of macro-synthetic fibers. Experimental results from pull-out tests were not available for the case of steel fibers used, so the pull-out curves are obtained with a numerical meso-model [30] that takes into account fiber geometry, location and orientation with respect to the crack plane and mechanical characteristics of the matrix.

A modified plastic damage model is used for concrete [24]. The plastic behavior is obtained as a generalization of classical theory of plasticity especially appropriate for geomaterials subjected to high confinement. The elastic behavior limit is defined using modified Lubliner–Oller yielding criterion [24]. Isotropic plastic hardening is used. The plastic hardening variable is obtained normalizing energy plastically dissipated to unity and varies between 0 for the virgin material and 1 when the material has dissipated all the available energy. The evolution law for the plastic

hardening variable takes into account the differentiated behavior in tension and compression. Evolution of the equivalent yielding threshold is defined taking into account the yielding thresholds evolution in uniaxial tension and compression tests and the actual stress state.

This concrete model is also used for asphalt concrete but with other material constants. Actually, asphalt concrete presents rate dependent and thermal effects that cannot be simulated with this model. This limitation was overcome using mechanical properties for asphalt concrete obtained from characterization tests made for similar strain rate and temperature to those used in the composite beams tests.

4. Numerical simulations and comparison with experimental results

4.1. Calibration of material properties

The models described in Section 3 were implemented in a 2D non linear finite element (FE) program developed for research purposes. First, the material mechanical properties were calibrated. For this purpose, characterization tests were numerically reproduced.

The concrete properties are indicated in Table 4. This concrete represents the plain concrete used as overlay and the matrix for both FRC overlays. The properties of the asphalt concrete substrate are also included in Table 4. The compressive strength and the modulus of elasticity were obtained from standard compression tests, the rest of the properties were indirectly adjusted to fit the experimental response obtained from notched beams tested under flexure.

The FE meshes used to simulate plain concrete compression and flexure tests are shown in Fig. 8. Plain stress four nodes elements with four Gauss points were used. In the case of flexure tests the mesh was refined near the notch.

The numerical response of plain concrete under uniaxial compression and flexure is presented in Fig. 9. Average experimental results are also included in Fig. 9b for comparison. Correlation between numerical and experimental results is obtained.

FE mesh used to simulate uniaxial compression test of asphalt concrete specimens is shown in Fig. 10a. A sensitivity analysis was performed to choose the appropriate mesh size. The numerical response of asphalt concrete under uniaxial compression and its comparison with experimental results are represented in Fig. 10b. A good agreement between numerical and a single experimental result is obtained with the same model used for concrete but using the parameters indicated in Table 4 for the asphalt concrete (Fig. 10b).

The mechanical properties of macro-synthetic fibers and steel fibers are presented in Table 5. Fiber pull-out tests results were used to define the fibers hardening behavior in axial direction. Force–displacement diagrams obtained from pull-out tests were used for the macro-synthetic fibers in axial direction, while a numerical meso-model was used to simulated the pull-out response of hooked-end steel fibers [30]. The corresponding load-displacement curves for macro-synthetic and steel fibers considering different fibers orientations are presented in Fig. 11. The embedded length of the fibers was taken as approximately 1/4 of the fiber total length that represents the average of all possible embedded lengths. For macro-synthetic fibers the experimental pull-out curve available corresponds to a fiber normal to the crack surface and with an embedded length of half the total fiber length. The curves corresponding to different orientations and an embedded length equal to 1/4 of the fiber total length were obtained extrapolating experimental results with the meso-model used for steel fibers but neglecting fibers flexure stiffness.

Taking into account the fibers length and the FRC beams dimensions [31,32] the estimated amount of fibers distributed in the vertical planes was 100% for macro-synthetic fibers and 80% of the total fiber content for steel fibers. For both fibers, this amount was distributed (see Fig. 12) 33% in axial direction, 33% inclined 60° with respect to axial direction and 33% forming an angle of −60° with axial direction.

The comparison between numerical and average experimental results for FRC beams bending tests is presented in Fig. 13. Numerical response can reproduce the bending hardening behavior making evident the change in the mechanical response with different fibers (Fig. 13). Although the peak load is almost the same, the residual strength obtained with steel fibers is markedly greater. In the case of steel fiber reinforced concrete experimental results present higher dispersion. This dispersion is typical of this material [22] and can be attributed to variations in fibers orientations. Some of the beams exhibited strain hardening following peak load. Numerical results describe an average experimental behavior for this case.

4.2. Numerical simulation of composite beams

Once the properties of all the materials used have been calibrated through the numerical simulation of characterization tests, the behavior of composite beams is numerically simulated. The FE mesh used is shown in Fig. 14. A sensitive analysis was performed to choose the mesh size. The different colors correspond to substrate and overlay. The substrate is always made of asphalt concrete. Plain concrete, steel fiber reinforced concrete and macro-synthetic fiber reinforced concrete are considered for the overlay.

Table 4
Plain concrete and asphalt concrete substrate properties.

Properties	Concrete overlays	Asphalt concrete substrate (20 °C)
Elasticity modulus E [MPa]	27,200	1,500
Poisson ratio v	0.2	0.2
Uniaxial compression yield threshold σ_{yc} [MPa]	25.0	0.2
Uniaxial compression strength σ_{uc} [MPa]	37.3	2.17
Uniaxial compression hardening curve	Exponential with maximum	Exponential with maximum
Crushing energy (hardening part) g_c [N mm/mm^3]	0.048	0.043
Crushing energy (softening part) G_c [N mm/mm^2]	8.0	3.50
Compression equibiaxial/uniaxial ratio R^{bc}	1.16	1.16
Parameter to control the shape of yield function in the octahedral plane [24] γ	3.5	3.5
Uniaxial tension elastic limit ratio σ_{yt} [MPa]	2.69	
Uniaxial tension strength σ_{uc} [MPa]	2.69	
Uniaxial tension hardening curve	Exponential decay	
Fracture energy (hardening part) g_f [N mm/mm^3]	0.0	
Fracture energy (softening part) G_f [N mm/mm^2]	0.09	

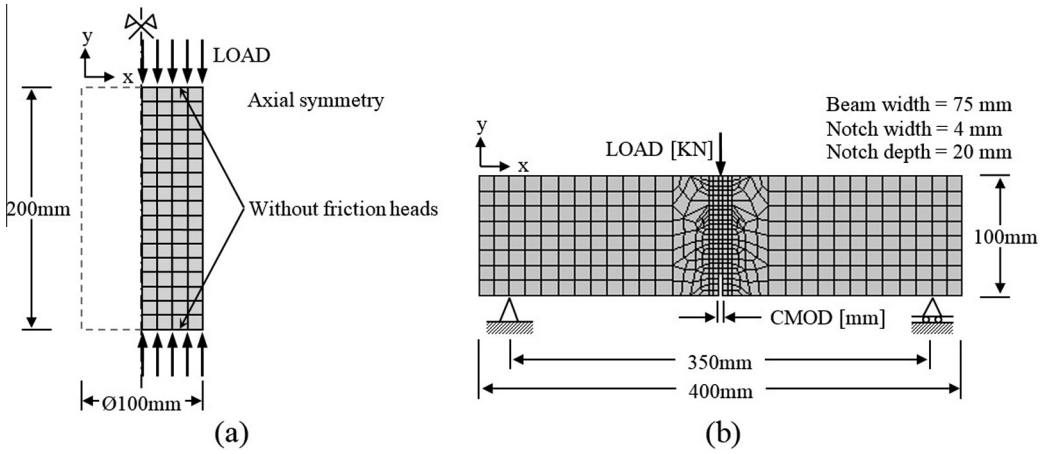

Fig. 8. FE mesh. (a) Uniaxial compression test; (b) flexure test.

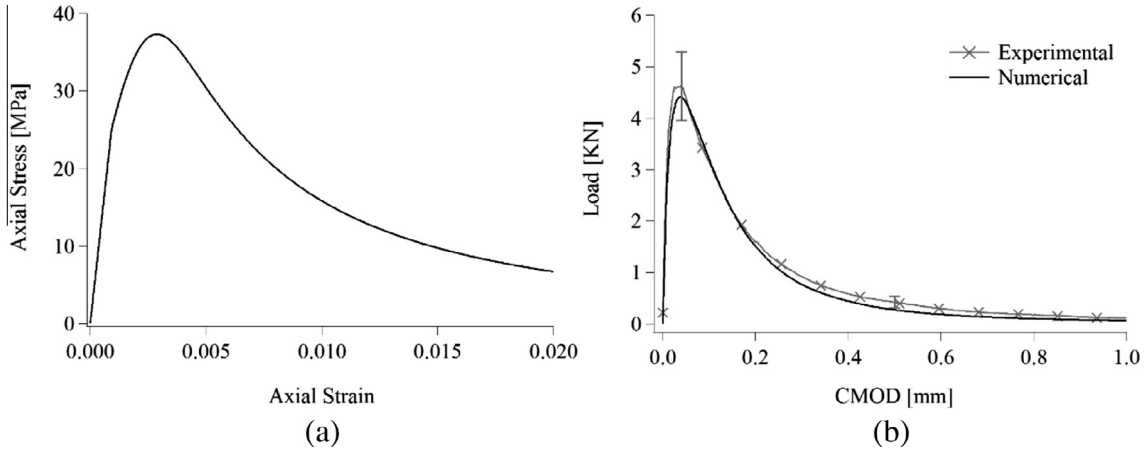

Fig. 9. Numerical response of plain concrete. (a) Uniaxial compression test; (b) flexure test.

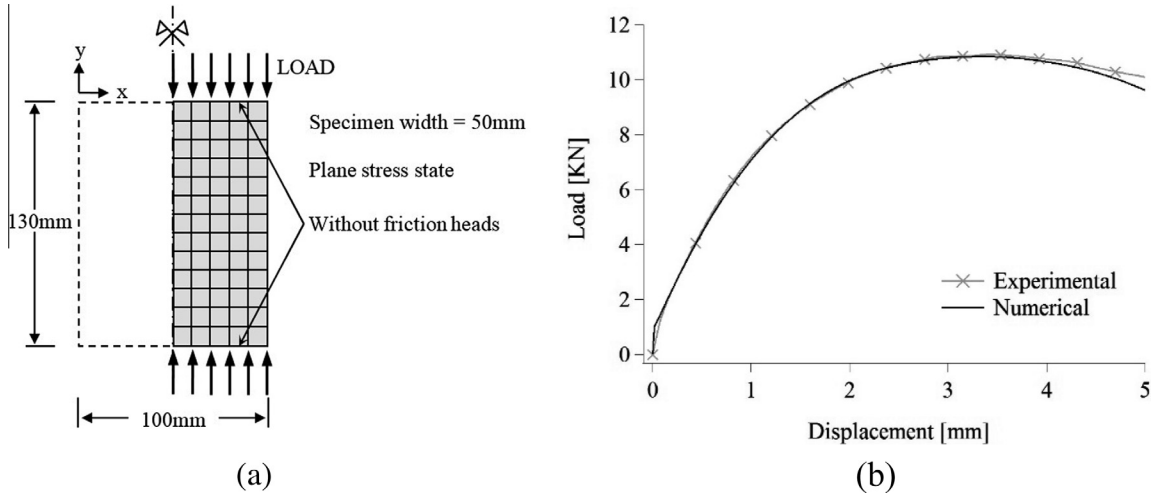

Fig. 10. Uniaxial compression test on asphalt concrete specimens. (a) FE mesh; (b) comparison of numerical and experimental results.

After the composite beams tests, some of the specimens were separated to analyze the actual fibers orientation in the overlays. The amount and orientation of fibers in the middle section was manually counted. In many papers it was shown that the fibers (both macro-synthetic and steel fibers) are mainly oriented in horizontal planes independently of the specimen height. In previous studies done by the authors ([31–34]) it was shown that the wall effect is very important and it favors the fiber orientation. In this study the relative small dimensions of the beams (400 mm long, 100 mm width and 50 mm height) forced the fibers in a major percentage in horizontal planes. The amount of fibers counted were supposed to be in horizontal planes distributed 33% in axial

Table 5
Fibers properties.

Properties	Macro-synthetic fibers	Steel fibers
Length [mm]	60	30
Embedded length [mm]	15	7.5
Diameter [mm]	0.84	0.38
Density [g/mm^3]	0.00091	0.008
Strength [MPa]	640	2,470
Elasticity modulus E_{xx} [MPa]	10,000	210,000
Poisson ratio $v_{xy} = v_{xz} = v_{zy} = v_{yz}$	0.2	0.2
Elasticity modulus $E_{yy} = E_{zz}$ [MPa]	1	1
Poisson ratio $v_{yx} = v_{zx}$	2.0×10^{-5}	9.52×10^{-7}
Slipping criteria and flaw	Von Mises	Von Mises
Slipping hardening	Fig. 11b	Fig. 11a
Slipping threshold ratio $\sigma_{fx}/\sigma_{fy} = \sigma_{fx}/\sigma_{fz}$	0.001	0.001
Direction x represents the axial fiber direction		

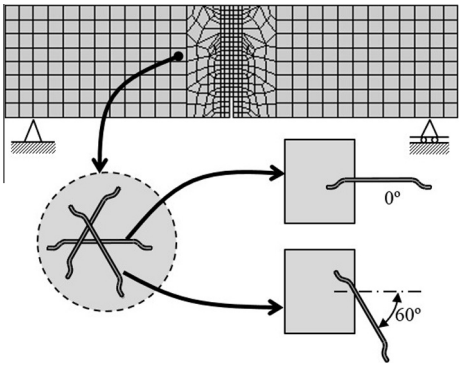

Fig. 12. Assumed fibers orientation.

direction, 33% inclined 60° with respect to axial direction and 33% forming an angle of −60° with axial direction.

Perfect adhesion between substrate and the overlay was assumed. The results of the numerical simulation of the corresponding composite beams and their comparison with experimental results are presented in Fig. 15.

The effect of adding different fibers to the overlay is captured by the numerical model that properly reproduces the experimental results. The numerical model assumes perfect bond between substrate and overlay in all cases, therefore the well concordance between numerical and experimental results suggests that although a crack along part of the interface was observed in some of the tests, this incipient debonding did not affect the structural response of the composite beams.

4.3. Other alternatives simulated

Once the numerical model was validated, different strengthening alternatives are numerically simulated and compared.

First, the effect of the same overlays but on a concrete substrate is studied and compared. The composite beams presented in Fig. 14 but with substrate made of Portland cement concrete are analyzed. The properties of the concrete substrate are assumed identical to those of the concrete matrix used for the overlay. The load displacement curves obtained for these composite beams with plain concrete, macro-synthetic fiber reinforced and steel fiber reinforced concrete overlay are presented in Fig. 16. The responses of the beams with asphalt concrete substrate are also included for comparison. Although the composite beams with concrete substrate have greater first peak strength than the composite beams with asphalt concrete substrate, the effect of adding fibers to the overlay is comparatively greater for the case of the asphalt concrete substrate. As an example, with the addition of macro-synthetic fibers the residual strength remains almost equal to the first peak load for asphalt concrete substrate and it strongly decreases for Portland cement substrate. For the case of 40 kg/m^3-·steel fiber overlay, the first peak load bearing capacity of the composite beam with asphalt concrete substrate is almost duplicated during the post peak, while for Portland cement concrete substrate the same addition of fibers is unable to increase the composite beam strength and the residual capacity becomes near 60% of the first peak.

The effect of different overlays applied to a same asphalt concrete substrate at different temperatures is also studied. The properties used for asphalt concrete in previous examples (Table 4) were obtained from characterization tests performed at room temperature (20 °C). Two different temperatures, one lower (5 °C) and one higher (35 °C) than room temperature are considered. This variation of temperature does not affect concrete mechanical properties. The effect of temperature on asphalt concrete mechanical properties was estimated from experimental results of compression tests made on asphalt concrete specimens at different temperatures. The modulus of elasticity and the compression strength of asphalt concrete were 6000 MPa and 6.0 MPa at 5 °C and 400 MPa and 1.0 MPa at 35 °C. The load-CMOD curves numerically obtained for PC-A, MFRC-A and SFRC-A composite beams at different temperatures are presented in Fig. 17. In all cases, following asphalt concrete properties tendency, the first peak strength

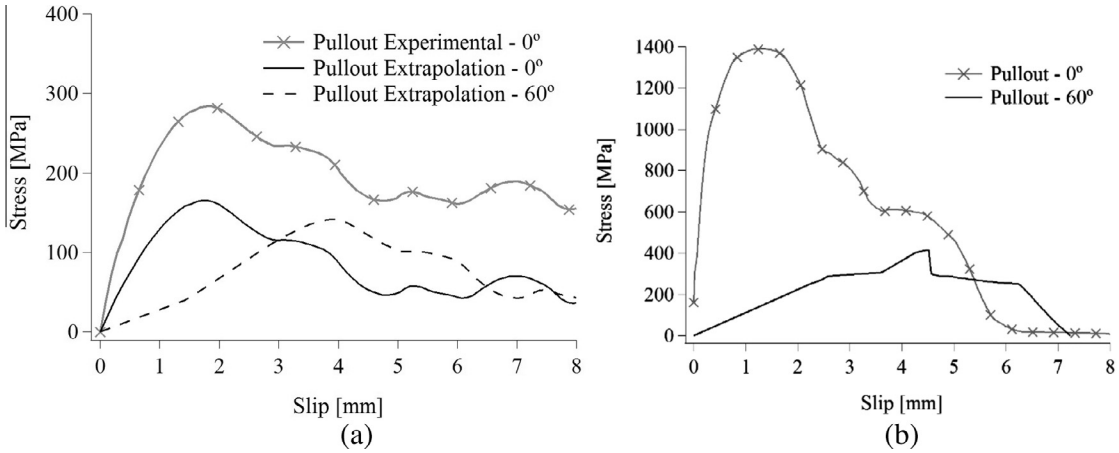

Fig. 11. Numerical results for pull-out tests with different inclination angles. (a) Macro-synthetic fibers. (b) Hooked end steel fibers.

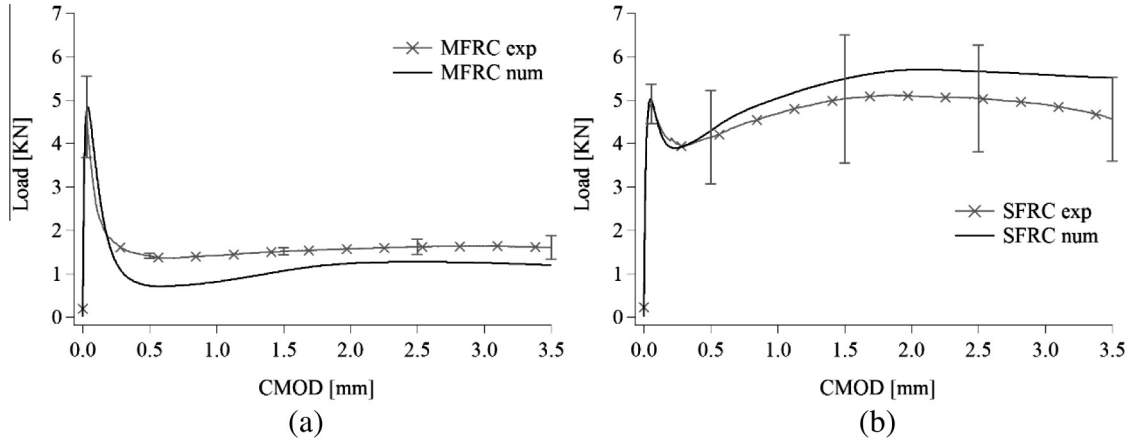

Fig. 13. Response of fiber reinforced concrete notched beams. Comparison of numerical and average experimental results. (a) MFRC; (b) SFRC.

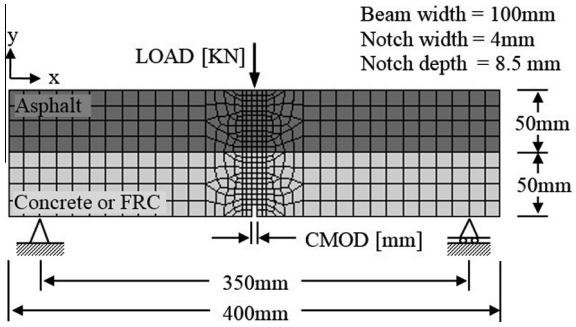

Fig. 14. FE mesh used for composite beams.

decreases with temperature but the variation from 5 °C to 20 °C is more pronounced than from 20 °C to 35 °C. For plain concrete overlay and macro-synthetic fiber reinforced overlay the residual strength is slightly affected by these variations in temperature; on the contrary, the numerical model indicates that the postpeak loading capacity of composite beams with steel fiber reinforced concrete overlay could be strongly reduced when the temperature increases from 20 °C to 35 °C.

Temperature affects asphalt concrete properties in different ways but both elasticity modulus and strength reduces with the temperature increase. For these reasons a better performance of the composite beams is obtained for the lowest temperature (5 °C) analyzed.

The effect of the dosage of fibers on the overlay is also numerically studied. The numerical results obtained for composite beams made of asphalt concrete substrate and macro-synthetic fiber reinforced concrete overlay and steel fiber reinforced concrete overlay with different fibers contents are presented in Fig. 18. It can be seen that 40 kg/m^3 of steel fibers are enough to increase load bearing capacity after the first peak, while more than 4.5 kg/m^3 of macro-synthetic fibers should be added to the overlay to increase composite beams strength. Both fibers dosages corresponds to a volumetric dosage of approximately 0.5%.

Finally, the effect of adding different fibers to the same overlay is also numerically studied. An overlay with 20 kg/m^3 of steel fibers and 3 kg/m^3 of macro-synthetic fibers (SMFRC) is analyzed. The numerical results corresponding to composite beams considering Portland cement concrete (PC) and asphalt concrete (A) as substrates are presented in Fig. 19, the case of concrete overlay with 40 kg/m^3 of steel fiber reinforcement (SFRC) is also included for comparison. It can be seen that the behavior of the composite beams with overlay including both fibers is similar to that with the steel fiber reinforced overlay with the advantage of reducing the amount of steel fibers and combining the beneficial effects of both fibers.

The application examples developed in this section show that the numerical model is useful for the mechanical behavior prediction of different whitetopping alternatives. It can be used as a design tool to choose the best overlay thickness, fibers type and content for each type and thickness of substrate.

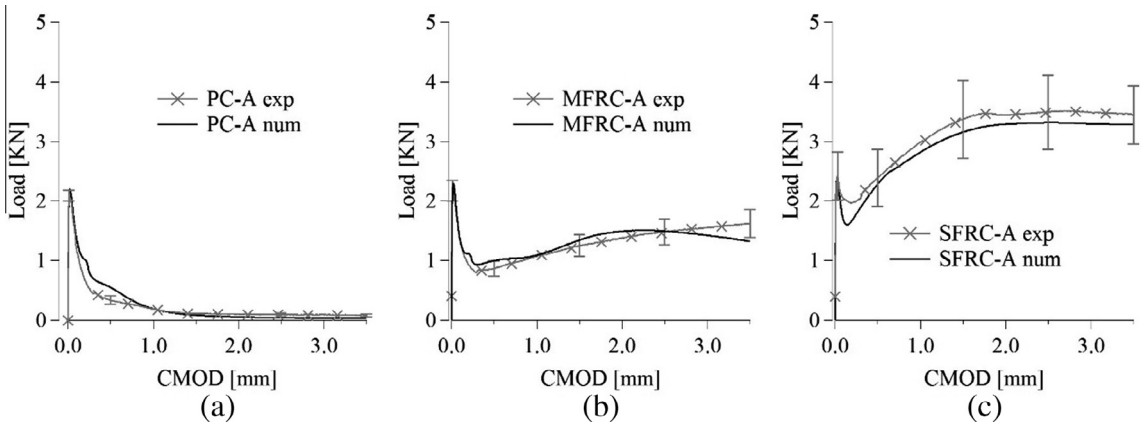

Fig. 15. Response of composite beams with asphalt concrete substrate. Comparison of numerical and average experimental results. (a) PC-A; (b) MFRC-A; (c) SFRC-A.

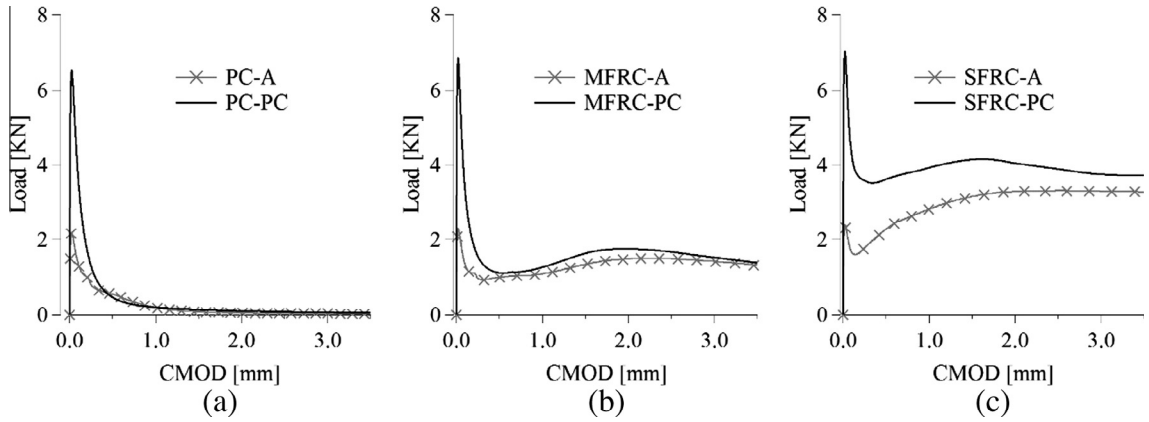

Fig. 16. Numerical response of composite beams with concrete substrate. Comparison with the case of asphalt concrete substrate. (a) PC overlay; (b) MFRC overlay; (c) SFRC overlay.

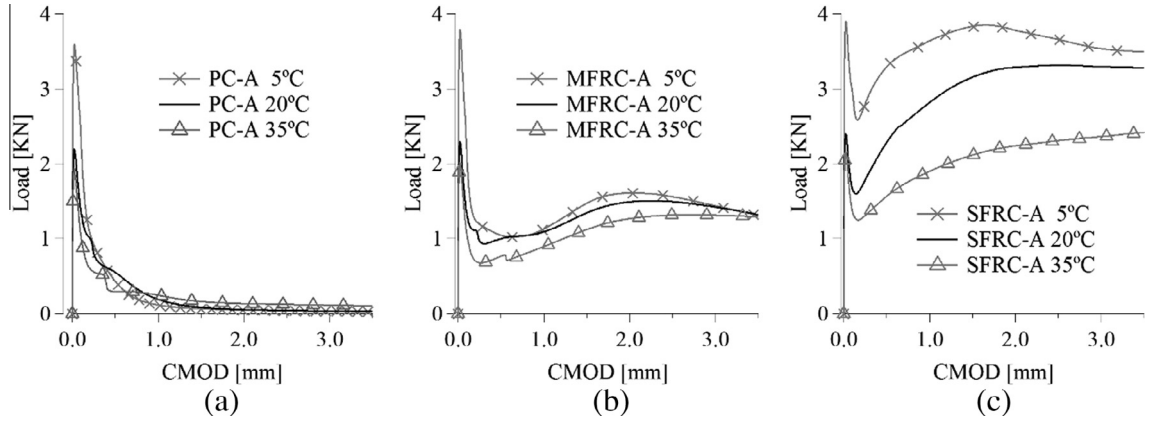

Fig. 17. Numerical response of composite beams at different temperatures. (a) PC-A; (b) MFRC-A; (c) SFRC-A.

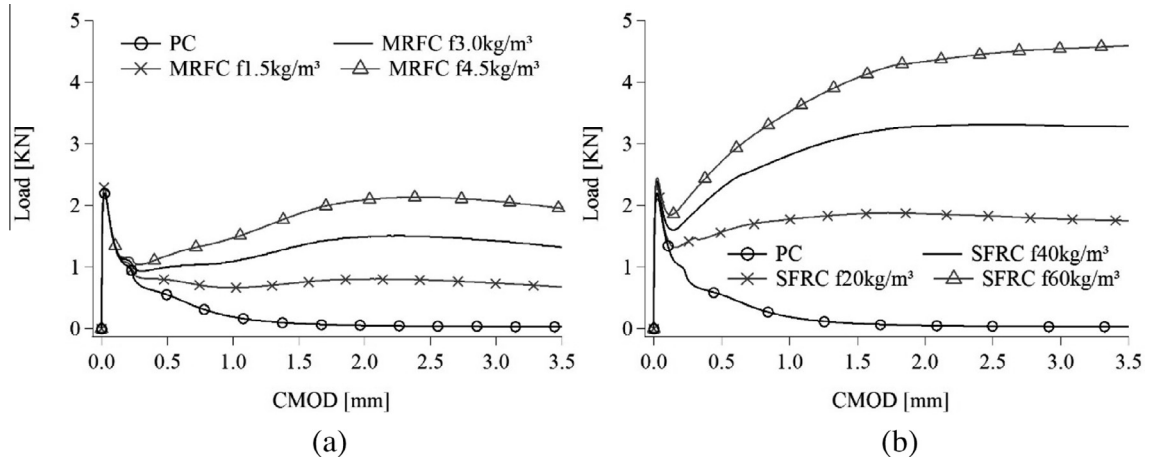

Fig. 18. Numerical response of composite beams of FRC-A with different fiber contents. (a) MFRC-A, (b) SFRC-A.

4.4. Numerical results analysis

The numerical model presented in Section 3 is used in this section to analyze the structural behavior of the composite beams numerically simulated in Sections 4.2 and 4.3. For this purpose, the axial strain and axial stress distributions along the central section of the composite beams are plotted in Figs. 20 and 21, respectively, for the different types of substrate and overlay analyzed.

Fig. 20 shows that, while the strain distribution is linear for the composite beams with concrete substrate, in the case of composite beams with asphalt substrate deformation distribution is no longer linear. In coincidence with experimental observations, for the composite beams with asphalt concrete substrate the advance of positive strains into the substrate is delayed. These facts explain the different behaviors observed in the cases of concrete substrate and asphalt concrete substrate.

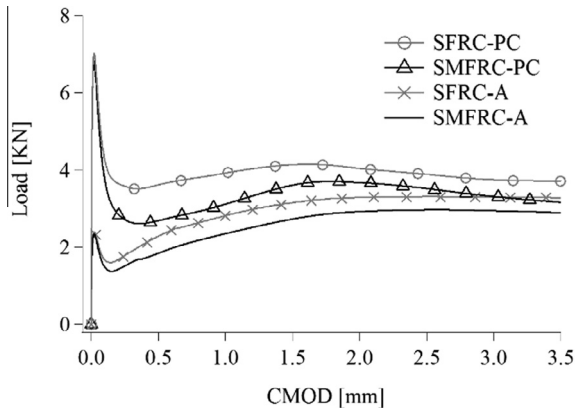

Fig. 19. Numerical response of composite beams made of asphalt concrete (A) and concrete (PC) substrates with SFRC and SMFRC overlay.

Moreover, Fig. 21 shows that the height of the compression zone is greater for the case of asphalt concrete substrate. The extension of the compression zone increases with the addition of fibers to the overlay and it is greater for the case of SFRC overlay than for the case of the MFRC overlay.

For these reasons, the structural behavior of composite SFRC beams depends more on the substrate properties than for the case of the composite MFRC beams. Thus, the differences between composite beams with asphalt concrete substrate and composite beams with concrete substrate are more pronounced for the case of SFRC overlays (Fig. 16c) than for the case of MFRC overlays (Fig. 16b). This fact also explains why the changes due to temperature in the structural behavior of the composite beams with asphalt concrete substrate are more pronounced for the case SFRC overlay (Fig. 17c) than for the case of MFRC overlay (Fig. 17b).

5. Conclusions

In order to study the mechanical response of fiber reinforced concrete overlays over asphalt concrete substrate three points bending tests on composite beams were performed. The overlay and the substrate are placed in the tension and compression zone respectively. The concrete overlay is notched to localize the failure and the crack opening rate is used to control the test.

The experimental methodology allowed the comparison and clear differentiation of the response of plain concrete overlays and concrete overlays reinforced with steel fibers and macro-synthetic fibers. For steel fiber reinforced concrete overlay,

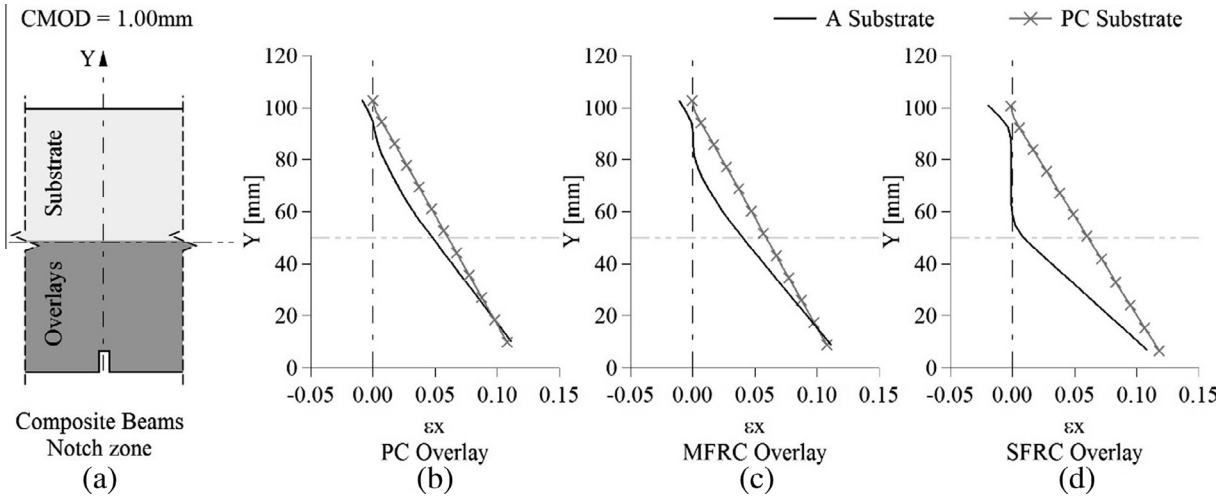

Fig. 20. Axial strain ε_x distribution in central section for CMOD = 1.00 mm. (a) Beams scheme; (b) composite beams with PC overlay; (c) composite beams with MFRC overlay; (d) composite beams with SFRC overlay.

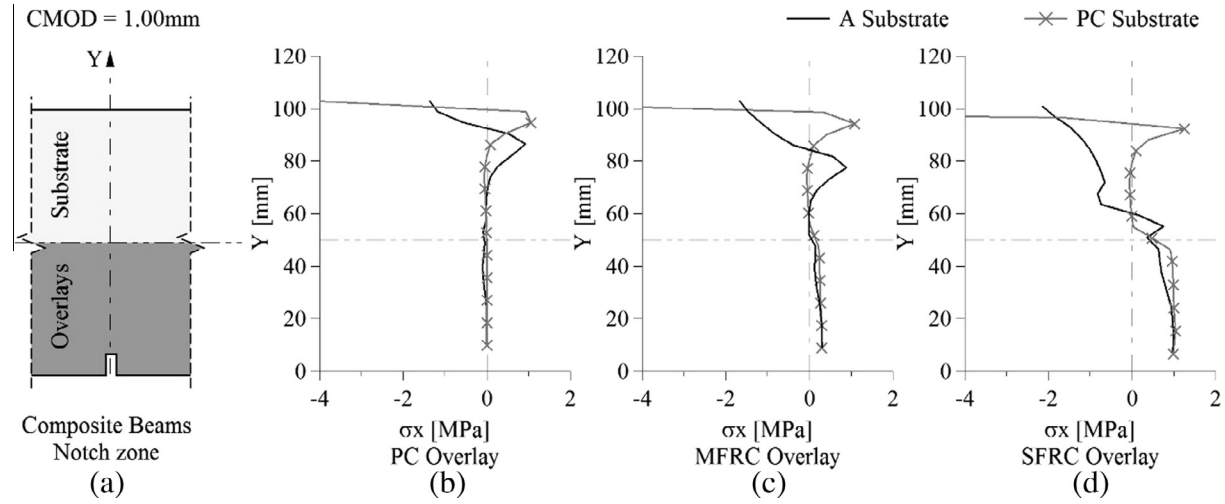

Fig. 21. Axial stress σ_x distribution in central section for CMOD = 1.00 mm. (a) Beams scheme; (b) composite beams with PC overlay; (c) composite beams with MFRC overlay; (d) composite beams with SFRC overlay.

the response of the composite beam (SFRC-A) was similar to that of the respective concrete beams (SFRC), but a greater increment in the residual capacity was observed. Unlike what happens in concrete beams, for macro-synthetic fibers overlay, the postpeak shows a progressive and very significant increase in residual capacity, which achieves almost 70% of the first crack load.

In addition to assessing the effect of using different types and fiber contents, the method could be used to compare different degrees of adherence at the substrate–overlay interface. Interface strength can be deteriorated due to many causes such as those caused by different roughness (scarification) or due to the lack of cleanliness of the substrate (a common field situation). The test configuration adopted seems suitable for evaluating the effect of strain rate, repeated load cycles, different frequency loads and temperature.

The experimental campaign presented in this paper corresponds to an exploratory campaign and no statistical inference work was done. Just descriptive statistics is reported in this paper. The present experimental study could lead to the design of a more complete campaign with a bigger number of specimens so that statistical inference could be done. It would be interesting to include in this future experimental campaign all the other alternatives that were only numerically simulated in this paper but have led to useful results.

A simple approach to model FRC was used to simulate the behavior of composite beams. Numerical results obtained with the assumption of perfect bond between substrate and overlay accurately reproduce the load-CMOD curves experimentally obtained evidencing that the interface cracks observed in some tests do not substantially affect structural behavior of the composite beams.

Addition of fibers to the overlay improves the behavior of the composite beams. The improvement is more marked in case of less resistant substrate.

Variation of asphalt concrete properties with temperature affects the peak strength of composite beams; the residual strength is almost independent of temperature for plain concrete and macro-synthetic fiber reinforced overlays and it appears more affected in the case of steel fiber reinforced concrete overlays.

Finally, the model predicts that a combination of steel and macro-synthetic fibers could lead to a similar mechanical behavior significantly reducing the amount of steel fibers.

The numerical tool developed is useful for the design of this type of intervention technique.

Acknowledgements

The authors wish to thank the financial support of LEMIT-CIC, National Scientific and Technological Research Council (CONICET) and National University of Tucumán research Council (CIUNT) and Ms. Amelia Campos for the English revision.

References

[1] National CP Tech Center. Guide to concrete overlays: sustainable solutions for resurfacing and rehabilitating existing pavements. 3rd ed. American Concrete Pavement Association Publication; 2014.
[2] National CP Tech Center. Institute for transportation. Guide to the design of concrete overlays using existing methodologies. Iowa: Iowa State University; 2012.
[3] Chunhua H. Synthesis of current Minnesota practices of thin and ultra-thin whitetopping. Minnesota Department of Transportation Report. 2005:43.
[4] Li Z, Dufalla N, Mu F, Vandenbossche J. Bonded concrete overlay of asphalt pavements mechanistic empirical design guide (BCOA-ME). Theory manual. Department of Civil and Environmental Engineering, University of Pittsburgh, Pittsburgh, Pennsylvania. 2013.
[5] Turatsinze A. Bonded cement-based material overlays for the repair, the lining or the strengthening of slabs pavements. RILEM State of the Art Reports. 2011.
[6] Ruano G, Isla F, Isas Pedraza R, Sfer D, Luccioni B. Shear retrofitting of reinforced concrete beams with steel fiber reinforced concrete. Constr Build Mater 2014;54:646–58.
[7] Turatsinze A, Granju J, Sabathier V, Farhat H. Durability of bonded cement-based overlays: effect of metal fibre reinforcement. Mater Struct 2005;38:321–7.
[8] Tran QT, Toumi A, Granju JL. Experimental and numerical investigation of the debonding interface between an old concrete and an overlay. Mater Struct 2006;39:379–89.
[9] Tran QT, Toumi A, Turatsinze A. Modelling of debonding between old concrete and overlay: fatigue loading and delayed effects. Mater Struct 2007;40:1045–59.
[10] Perez F, Bissonnette B, Gagne R. Parameters affecting the debonding risk of bonded overlays used on reinforced concrete slab subjected to flexural loading. Mater Struct 2009;42:645–62.
[11] Tayeh BA, Abu Bakar BH, Megat Johari MA. Characterization of the interfacial bond between old concrete substrate and ultra high performance fiber concrete repair composite. Mater Struct 2013;46(5):743–53.
[12] Rasmussen RO, Rozycki DK. NCHRP synthesis of highway practice 338: thin and ultra-thin whitetopping. Washington, D.C.: Transportation Research Board, National Research Council; 2004.
[13] Cervantes V, Roesler J. Performance of concrete pavements with optimized slab geometry. Research Report ICT-09-053, Illinois Center for Transportation ISSN: 0197–9191. University of Illinois at Urbana-Champaign; 2009.
[14] Bordelon AC, Roesler JR. Desing with fiber-reinforcement for thin concrete overlays bonded to asphalt. ASCE J Transp Eng 2012;138:430–5.
[15] EN 12697–33. Bituminous mixture: test methods for hot mix asphalts, Part. 33: specimen prepared by roller compactor. 2003.
[16] EN 14651–33. Test method for metallic fibered concrete – measuring the flexural tensile strength (Limit of proportionality (LOP), residual). 2005:18.
[17] Giaccio G, Tobes JM, Zerbino R. Use of small beams to obtain design parameters of fibre reinforced concrete. Cement Concr Compos 2008;30(4):297–306.
[18] Giaccio G, Bossio ME, Monetti DH, Torrijos MC, Zerbino R. Macrofibras sintéticas para el refuerzo de hormigón. Segundas jornadas de investigación y transferencia. FI-UNLP. 2013:330–5.
[19] Mesbah HA, Kassimi F, Yahia A, Khayat H. Flexural performance of reinforced concrete beams repaired with fiber-reinforced SCC. In: Fifth Intnl. RILEM Symp. On Self Compacting Concrete. 2000.
[20] Martinola G, Meda A, Plizzari GA, Rinaldi Z. Strengthening and repair of RC beams with fiber reinforced concrete. Cement Concr Compos 2010;32:731–9.
[21] Blanco A, Pujadas P, de la Fuente A, Cavalaro S, Aguado A. Application of constitutive models in European codes to RC–FRC. Constr Build Mater 2013;40:246–59.
[22] Luccioni B, Ruano G, Isla Calderón F, Zerbino R, Giaccio G. A simple approach to model SFRC. Constr Build Mater 2012;37:111–24.
[23] Luccioni B, Oller S, Danesi R. Coupled plastic damage model. Comput Methods Appl Mech Eng 1996;129:81–9.
[24] Luccioni B, Rougier V. A plastic damage approach for confined concrete. Comput Struct 2005;83:2238–56.
[25] Luccioni B, López DE. Modelo para materiales compuestos con deslizamiento de fibras. Análisis y cálculo de estructuras de materiales compuestos. 2002:411–31.
[26] Truesdell C, Toupin R. The classical field theories. Handbuch der Physik. 1960.
[27] Lubliner J. On the thermodynamic foundations of non-linear mechanics. Int J Non Linear Mech 1972;7:237–54.
[28] Luccioni BM, López DE, Danesi RF. Bond-slip in reinforced concrete elements. J Struct Eng 2005;131(11):1690–8.
[29] Betten J. Application of tensor functions to the formulation of yield criteria for anisotropic materials. Int J Plast 1988;4:29–46.
[30] Isla F, Luccioni B. Rotura de fibras en hormigones reforzados con fibras. Mecanica Computacional 2013;32:333–54.
[31] Torrijos MC, Barragán B, Zerbino RL. Placing conditions, mesostructural characteristics and post-cracking response of fibre reinforced self-compacting concretes. Constr Build Mater 2010;24(6):1078–85.
[32] Zerbino R, Tobes JM, Bossio G. On the orientation of fibres in structural members fabricated with self compacting fibre reinforced concrete. Cement Concr Compos 2012;34(2):191–200.
[33] Torrijos MC, Giaccio G, Zerbino R. Transport properties in cracked fiber reinforced concrete. In: 8th RILEM International Symposium on Fiber Reinforced Concrete: challenges and opportunities (BEFIB 2012). 2012:680–91.
[34] Isas R, Torrijos M, Giaccio G, Zerbino R, Luccioni B, Sfer D. Hormigones autocompactantes con fibras: respuesta mecánica de losas sometidas a cargas puntuales y vigas delgadas. BAC2010, Segundo Congreso Iberico Sobre Hormigon Autocompactable. 2010:125–35.